Online waveform processing for demanding target situations

Martin Pfennigbauer*, Clifford Wolf, Josef Weinkopf, Andreas Ullrich
RIEGL Laser Measurement Systems GmbH, Riedenburgstrasse 48, 3580 Horn, Austria

ABSTRACT

RIEGL LIDAR instruments are based on echo digitization and provide point cloud data by online waveform processing or full waveform data for external full waveform analysis or both. The advantages of online waveform processing of being fast and highly accurate for most typical target situation are made up by full waveform processing for demanding echo signal shapes when employing sophisticated algorithms. It is investigated how online waveform processing performs in turbid media and where the limitations are by analyzing experimental results when measuring in a fog chamber. An algorithm is proposed to determine the visibility range from the echo waveforms return of the medium.

Keywords: laser scanning, echo digitization, online waveform processing, fog penetration, atmospheric attenuation, visibility range

1. INTRODUCTION

Since its introduction about 15 years ago, laser scanning now has become a standard method in surveying. LIDAR instruments for terrestrial, mobile, and airborne applications are frequently employed under adverse atmospheric conditions. Clouds, fog, precipitation, or dust might cause these. Prominent examples are the application in industrial environments, for mining, or shipping. The necessity to penetrate an atmosphere with significant backscatter and attenuation arise from the desire to be able to still perform accurate surveying, reliable surveillance, or hazard avoidance of moving platforms.

Under such conditions the instruments face certain difficulties. First of all the signal from a target is weakened by the increased atmospheric attenuation. Second, distributed reflectance from the atmosphere may be erroneously interpreted as echo signal from a target. Third, a true target might be discarded due to wrong assessment of its reflectance because of unknown atmospheric conditions.

It is therefore desirable to have a strong laser and a sensitive receiver with sufficient power margin to overcome the atmospheric attenuation as well as a powerful signal analysis to be able to detect target echoes in the presence of signals from the medium the laser beam is travelling through. Furthermore it would be of great advantage to be able to estimate atmospheric properties in order to properly take into account their effects on the actual measurement results.

RIEGL has long been successful in developing, manufacturing, and marketing of laser scanning instruments and systems employing pulsed time-of-flight measurement with echo digitization for multiple purposes. Turnkey solutions for airborne, mobile, and terrestrial laser scanners employing full waveform processing as well as the associated software tools have now been available on the market for more than 10 years [1]. About 5 years ago, online waveform processing has been introduced [2], [3] complementing full waveform analysis with certain advantages like improved accuracy and efficiency but limitations with respect to dealing with overlapping pulses resulting from multi-target situations. The question addressed in this paper is how the different technologies can cope with demanding target situations, namely when measuring through or into scattering and attenuating media. Enhancing online waveform processing by measuring the relative pulse broadening provide additional attributes [4], support target classification and improve measurement accuracy for targets resulting from distributed reflection [5],[6]. It is now assessed what improvements can be gained from further analysis of echo signals potentially originating from fog of varying density.

* mpfennigbauer@riegl.com; phone 43 2982 4211; fax 43 2982 4210; www.riegl.com

Martin Pfennigbauer, Clifford Wolf, Josef Weinkopf, Andreas Ullrich,
"Online waveform processing for demanding target situations“, in Proc. SPIE 9080-18, 2014.

In this paper we present measurement results obtained with a *RIEGL* VZ-1000 in a fog chamber. The results obtained with unmodified online waveform processing are analyzed and it is assessed how dedicated algorithms for online waveform processing or full waveform analysis might improve the capability to penetrate such media. The paper is organized as follows: after a brief introduction on the employed sensor technology we present the experimental setup and the obtained results. Enhanced algorithms for online waveform processing and full waveform analysis are proposed and the potential consequences are analyzed.

2. MODELLING THE SENSOR'S INTERACTION WITH MEDIUM AND TARGET

Pulsed time-of-flight laser ranging is based on the emission of laser pulses, which interact with a target, and the detection of echo signals collected by the receiver aperture and converted into an electrical signal. A corresponding block diagram is presented in Figure 1. The time it takes the laser pulse to travel from the instrument to the target and the echo signal to return to the instrument is measured and the corresponding range is calculated.

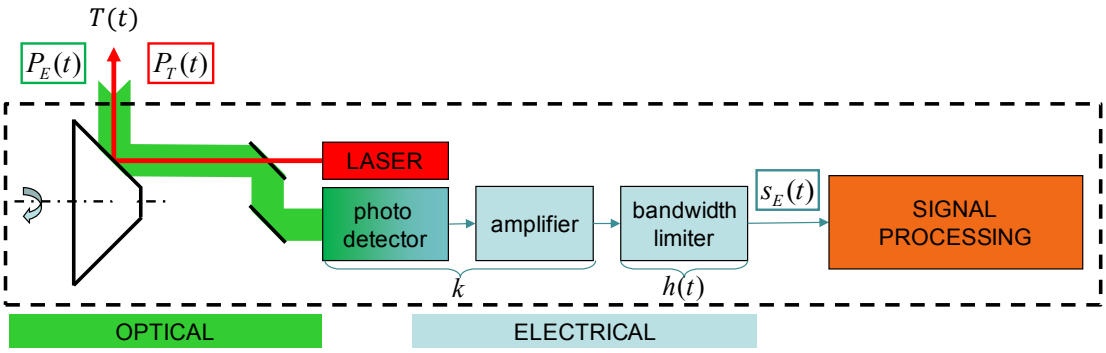

Figure 1: Block Diagram LIDAR Instrument

The interaction at the target is mathematically described as a convolution of the laser pulse shape $P_T(t)$ and the target signature $T(t)$

$$P_E(t) = P_T(t) * T(t) \tag{1}$$

At the receiver the process of transforming the optical signal into an electrical signal used for time measurement is represented by multiplication with the optical-to-electrical conversion factor k and a convolution with the impulse response of the receiver $h(t)$

$$s_E(t) = kP_E(t) * h(t) = k(P_T(t) * T(t)) * h(t) \tag{2}$$

The commutativity of the convolution allows us to rearrange Eq. (2) as follows:

$$s_E(t) = \underbrace{kP_T(t) * h(t)}_{\text{system response}} * T(t) = s_R(t) * T(t) \tag{3}$$

where the laser pulse shape and the impulse response of the receiver are interpreted as system response $s_R(t)$. The shape of the received signal thus is the convolution of the known system response and the unknown target impulse response or target signature.

For a target opaque for the laser's wavelength, the target signature is determined by the target's reflection properties (reflectivity and directivity), size, shape, and orientation with respect to the laser beam. Whenever the interaction between the laser pulse and the target occurs within a single instant, or, in other words, when a target's temporal extent is zero, the target signature is the Dirac delta function scaled with the laser radar cross section (LRCS) [7].

Online waveform processing relies on the implicit assumption that every received echo signal is the result of the laser pulse hitting a target of which the signature is the Dirac delta function and the backscatter cross section a:

$$s_E(t) = s_R(t) * T(t) = s_R(t) * a\delta(t_0) = as_R(t - t_0). \tag{4}$$

Based on this assumption, every digitized echo signal is compared to the previously determined system response ("system response fitting") [8]. This approach gives the utmost accuracy and precision which can be achieved in an

echo-digitizing LIDAR system and also perfectly accounts for effects imposed by non-linear signal compression. Online waveform processing has its limitations when superposition of signals from nearby targets is present. Due to the lack of computational power in real-time processing the rigorous approach of LSQ-Fitting of numerous superimposing responses cannot be applied. In such cases other algorithms like rigorous approaches aiming at the deconvolution [9] and approaches based on modeling the digitized echo waveforms by means of basic functions, e.g. Gaussian decomposition, give superior results [8][10]. However, online waveform processing at least informs the user about the merging of target responses by providing information on the deviation of the actual target's pulse shape from the expected pulse shape [1].

Targets with a certain spatial (or temporal) extent are described by functions other than the Dirac function. The example of discrete but slanted targets has been thoroughly discussed in [5]. In this paper we want to investigate the effect of turbid media with distributed reflectance like fog, dust clouds, or turbid water.

The signature of the medium in such a case might generally be modeled as

$$T(t) = a\delta(t_0) + b\sigma(t - t_0)e^{-(t-t_0)/\tau}, \tag{5}$$

when we assume a homogeneous medium, i.e., the backscatter coefficient and the attenuation are constant inside the medium. The first part constitutes the portion of diffuse or specular reflection (backscatter cross section a) when entering the turbid medium at instant $t = t_0$ (this could be the water surface or window pane of a fog chamber in an experimental setup). The second part represents the distributed reflectance inside the medium, starting at $t = t_0$. With the penetration depth τ and the backscatter factor b. For the analyses presented here, the first part is not applicable as the measurements have been performed with the instrument *inside* the turbid medium. Hence the echo signal reads

$$s_E(t) = s_R(t) * T(t) = s_R(t) * b\sigma(t - t_0)e^{-(t-t_0)/\tau} \tag{6}$$

3. EXPERIMENTAL SETUP

The experiments have been performed in a fog chamber at the test site Laboratoire régional des Ponts et Chuassées de Clermont-Ferrand in France, with a *RIEGL* VZ-1000 in March 2014. Figure 2 shows a sketch of the experimental setup: The target distance was about 30 m, both instrument and targets were in fixed positions. The instrument was operated at a laser pulse repetition rate of 70 kHz in line scanning mode at a line rate of 2.5 lines per second. The target was a flat board covered with black and white plaster oriented roughly perpendicular to the laser beams as indicated in Figure 2. The surface was designed in such a way to have reflection properties close to a perfect Lambertian reflector. The reflectance of the black and white surface was determined to be 3% and 100% at the laser wavelength, respectively. The instrument was controlled with a laptop computer from a detached room outside the fog chamber.

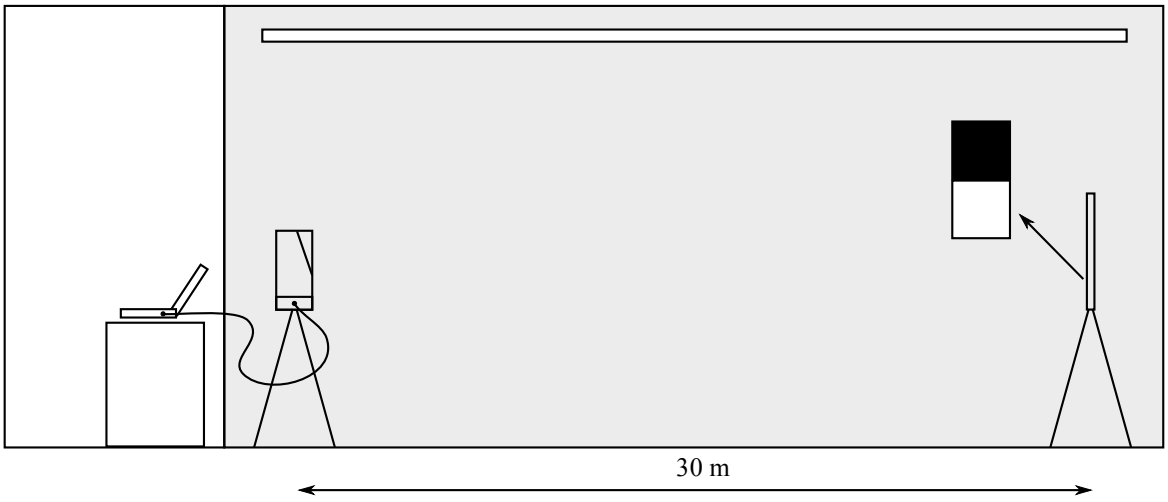

Figure 2: Experimental setup.

The fog chamber could produce temporally stable and spatially homogenous fog in a wide range of densities. The artificial fog was generated by sprinkling small water droplets from pipes located at the ceiling of the chamber. The density of the fog was controlled and quantified on site by determining the visibility range (i.e. the range at which the

contrast between a perfectly black and a perfectly white target is 2%) and maintaining the desired value by means of the fog generators. Figure 3 gives a visual impression of the fog chamber. The results of the measurements were

- the point cloud gained by the instrument's online waveform processing,
- the associated waveforms as stored when using the optional full waveform output option, and
- waveform data with a significantly increased size of the acquisition window of sampling values compared to the conventional waveform output.

The latter sort of waveform data is currently not available for the user. Apart from this special setting, the *RIEGL* VZ-1000 instrument was a standard production unit.

Figure 3: Visual impression of the fog chamber.

4. EXPERIMENTAL RESULTS

The following questions are investigated on basis of the data acquired during the experiments:

- How does standard online waveform processing work under adverse atmospheric conditions?
- Can echo signals from fog be identified as such?
- How good is the penetration of fog?
- Can modified algorithms improve the target attributes?

As mentioned in the previous section, the target board was scanned in line scan mode from top (black section) to bottom (white section). In Figure 4 measurement results are illustrated by presenting the attributes of the points of the point cloud over the line scan angle for three fog densities, i.e., different visibility ranges. The top diagram shows the range readings, the second and third diagram provide the corresponding amplitude and reflectance value, respectively. The bottom diagram indicates the pulse shape deviation. The color of the points indicates the number of the corresponding target in the range gate.

The results without fog serve as reference as there are only measurements from the target board at about 30 m. Mean and standard deviation of the range measurements are 29.4280 m and 2.7 mm for the black section and 29.4295 m and 1.7 mm for the white section of the target board. The amplitude readings are about 25 dB for black and about 40 dB for white. The corresponding relative reflectance values are -15 dB (3.2% reflectance) and 0 dB (100% reflectance). The pulse shape deviation is below 10 for both targets as would be expected from a flat target under these measurement conditions.

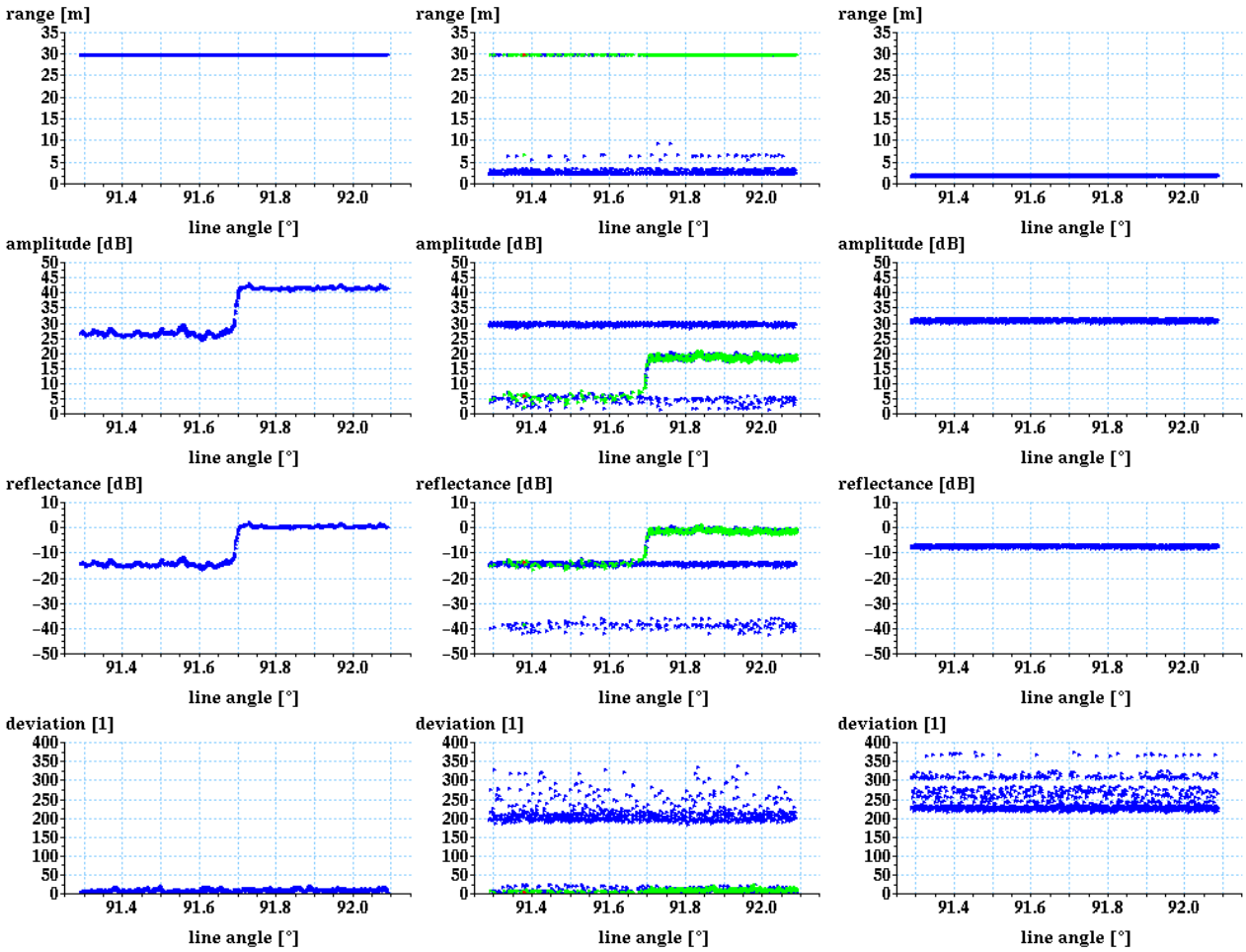

Figure 4: Measurement results without fog (left column), at 40 m visibility (middle column), and at 10 m visibility (right column). The color indicates the number of the target in the range gate. Blue refers to first targets, green to second targets and red to third targets.

The results are quite different in the presence of dense fog (40 m visibility): There are again points at 30 m originating from the target board but now also measurements at a shorter distance which are attributed to echoes from the fog. In the presented example there is a fog echo at about 2.5 m almost for every single measurement. These fog echoes have high amplitudes of about 30 dB where the echo amplitude from the board is reduced by about 20 dB due to the attenuating effect of the fog. The reflectance readings of the measurements from the target board are not affected by the fog, as the atmospheric attenuation, derived from the know visibility range, has been correctly taken into account. Note that the relative reflectance of the fog is about the same as it is for the black target while its amplitude is higher than the white target. There is a second sparsely populated layer of echoes from the fog at about 7 m with considerably lower amplitude. All fog echoes have in common a considerably increased pulse shape deviation of about 200 and higher. This property can be used to distinguish fog echoes from true target readings. As a direct consequence it puts the user into the position to eliminate false targets from turbid media by applying a deviation filter already with an unmodified *RIEGL* VZ-1000.

With very dense fog (10 m visibility), the atmospheric attenuation is too high to permit measuring to the board at 30 m distance. All targets detected originate from the fog at a very close range, with high amplitude and still high pulse shape deviation. The amplitude and also the reflectance of the fog targets are higher than in the case of 40 m visibility. Furthermore it is worth mentioning that in case of such dense fog there is only a very distinct layer causing echoes and no measurements are triggered from further within the fog due to its high attenuation and distributed backreflection.

The waveforms for the three different measurement conditions discussed above are presented in Figure 5. The small echo signal present in the vicinity of the instrument (at $t = 0$) in the absence of fog is caused by the exit window pane of the instrument. The figure gives the waveforms for the entire line scan, hence waveforms for black target and white target are shown as well as intermediate echo signal strengths when the laser beam hits both targets. This is particularly good to be seen in absence of fog. For 40 m visibility the fog echo has a considerable amplitude (higher than the white target echo, see discussion above). For 10 m visibility there is no echo at all from the target board whereas the fog echo waveform has a shape that would, after taking into account the nonlinearity of the receiver, neatly follow the theoretical expectation from Equ. (6).

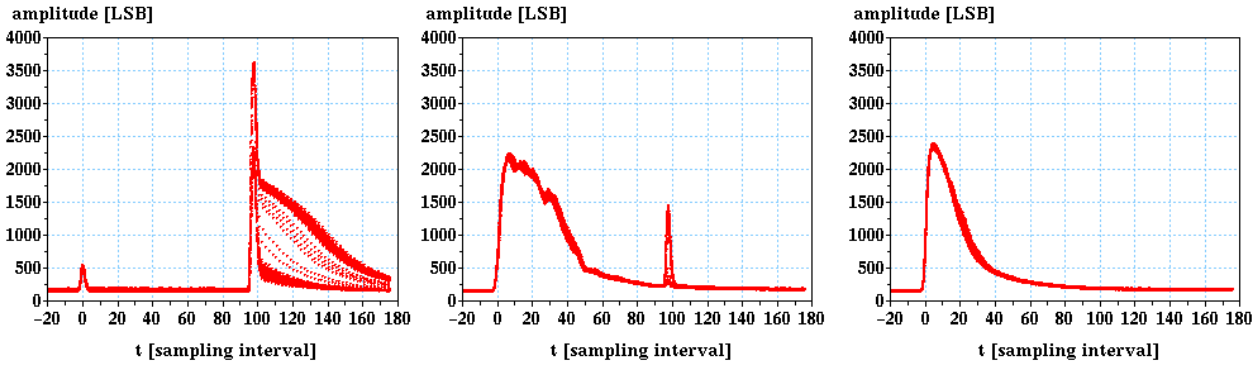

Figure 5: Echo waveforms without fog (left), at 40 m visibility (middle), and at 10 m visibility (right).

In order to determine the relative reflectance, not only the near range sensitivity of the instrument [3] and the $1/R^2$ law from laser radar range equations [12] have been taken into account but also the atmospheric attenuation. The figures in [13] have been used as a starting point to determine the atmospheric attenuation. From there the value of the atmospheric attenuation σ in units 1/m as a function of the visibility V in units of m is σ=2.25/V. This value, however, applies for rather clear conditions with visibility ranges between 3 km and 60 km. By comparing the results obtained during our experiments at comparatively extremely low visibility ranges, a value of σ=3.6/V proved to be the best fit in order to obtain correct and constant reflectance readings. Hence the relative reflectance for a target at distance R at a visibility range V is calculated through

$$\rho_{\mathrm{rel}} = A_{\mathrm{dB}} - A_{\mathrm{dB,ref}}(R) + 3.6\frac{R}{V}\frac{10}{\ln(10)}, \qquad (7)$$

with the target's amplitude A_{dB}, the range-dependent amplitude $A_{\mathrm{dB,ref}}(R)$, obtained during instrument calibration [3], and the factor 10/ln(10) following from the transition from 1/km to dB/km of the atmospheric attenuation.

Mean amplitude and reflectance values for black and white targets as well as the mean deviation readings for the targets triggered by the fog is given in Table 1 for all visibility ranges investigated in the course of the experiments. In Figure 6 the corresponding results are illustrated in a compound graph. It is unclear why measurements to the white target were not possible at 20 m visibility range where one would expect around 6 dB amplitude when extrapolating the other results.

Table 1: Summary of the experimental results.

visibility	amplitude white paper	reflectance white paper	amplitude black paper	reflectance black paper	deviation fog
[m]	[dB]	[dB]	[dB]	[dB]	[1]
10	-	-	-	-	226
20	-	-	-	-	221
30	12	2	-	-	214
40	18	0	5	-13	200
50	22	-1	10	-14	61
60	30	2	15	-10	13
no fog	41	0	26	-15	-

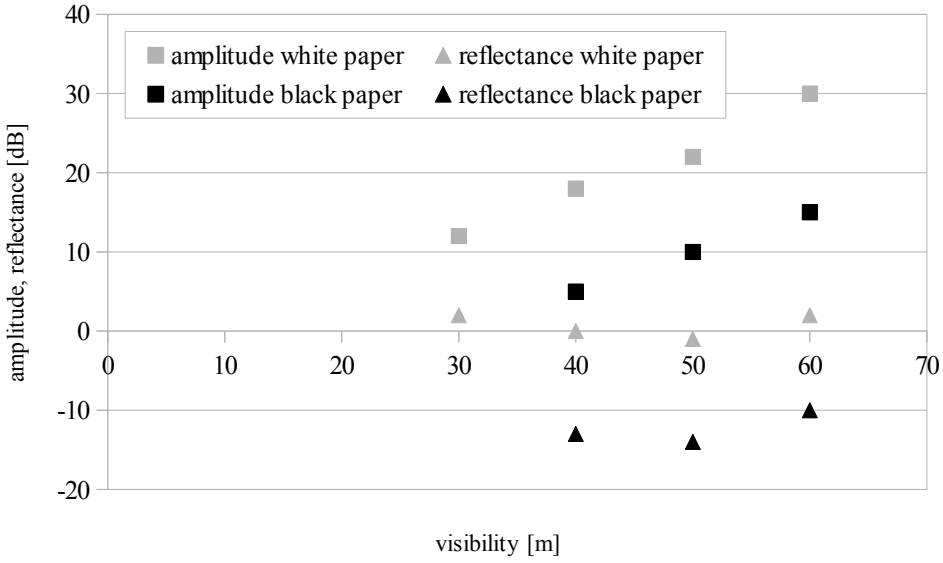

Figure 6: Amplitude and reflectance readings (squares and rectangles) for black and white targets (black and grey) as a function of the visibility in the fog chamber.

5. ANALYZING THE FOG ECHO SIGNAL

We now want to take a closer look at the echo waveform the instrument receives from the distributed reflection of the medium. In the previous section it has already been pointed out that these echoes have a significantly higher pulse shape deviation than echoes from true targets. (Certainly there are cases where overlapping echoes from multiple targets may also result in increased pulse shape deviations. One common example would be measuring into vegetation.) With conventional online waveform processing only a very limited number of sampling values is analyzed but we have already seen that the distributed echo from the fog has considerable length (cf. Figure 5). If we want the echo targets not merely be discarded but actually analyzed, different approaches have to be investigated.

In Figure 7 a total of about 1,000 waveforms from the fog for different visibility ranges are plotted over time. These waveforms are modified compared to the ones shown in Figure 5 by now taking into account both the receiver nonlinearity and the range variation of the sensitivity of the instrument. These two dependencies are properties of the instrument which are determined during calibration. Applying these corrections makes it possible to compare the echo waveform's shapes from fog of different density with the aim to determine the visibility range.

Determination or at least estimation of the visibility range associated to a layer of turbid medium is desirable for several reasons. First, knowledge about the atmosphere's attenuation puts one in the position to correctly determine the relative reflectance of targets within or behind such a layer. As a consequence of this the information might be used to apply correct detection thresholds for target detection, which reduces the risk of disregarding targets producing just a weak echo signal. Furthermore comparing the waveform to typical shapes might give improved evidence of a waveform actually originating from distributed backscattering.

It is obvious that in our experiments the waveforms from the fog, especially for larger visibility ranges (>30 m) do not show the exponential decay as for low visibility range. Furthermore, the waveforms become less stable and tend to show multiple local maxima. This may possibly be attributed to the fact that the artificial fog generated in the chamber is less homogeneous or less evenly distributed when the fog's density is comparatively low. If the same would be the case for natural fog cannot be deduced from the setup employed here and is subject to further investigations.

Nevertheless it seems possible to find a measure for the visibility range from the waveform. One approach would be to determine the temporal distance D_{COM} of the position of the center of mass T_{COM} of the fog waveform from the position of the rising edge T_{re}

$$D_{\mathrm{COM}} = T_{\mathrm{COM}} - T_{\mathrm{re}} = \frac{\sum t_i s_i}{\sum s_i} - T_{re}, \tag{8}$$

where s_i and t_i are the sampling values and the sampling instances, respectively and T_{re} is defined as the instant where the pulse reaches its half-peak value.

This distance can be expressed in sampling intervals or in meters. The main point is that with the abovementioned corrections applied to the waveform the actual value does not depend on the distance from the instrument. If for example there is a dust cloud at a certain distance from the instrument D_{COM} can still be calculated in the same way. Figure 8 shows the resulting scatterplot for D_{COM} over the visibility range. As might be expected from the waveforms, the uncertainty grows with increasing visibility. The red curve corresponds to the mean values of D_{COM} which might be used in tabulated form to estimate the visibility range in real time from echo waveforms.

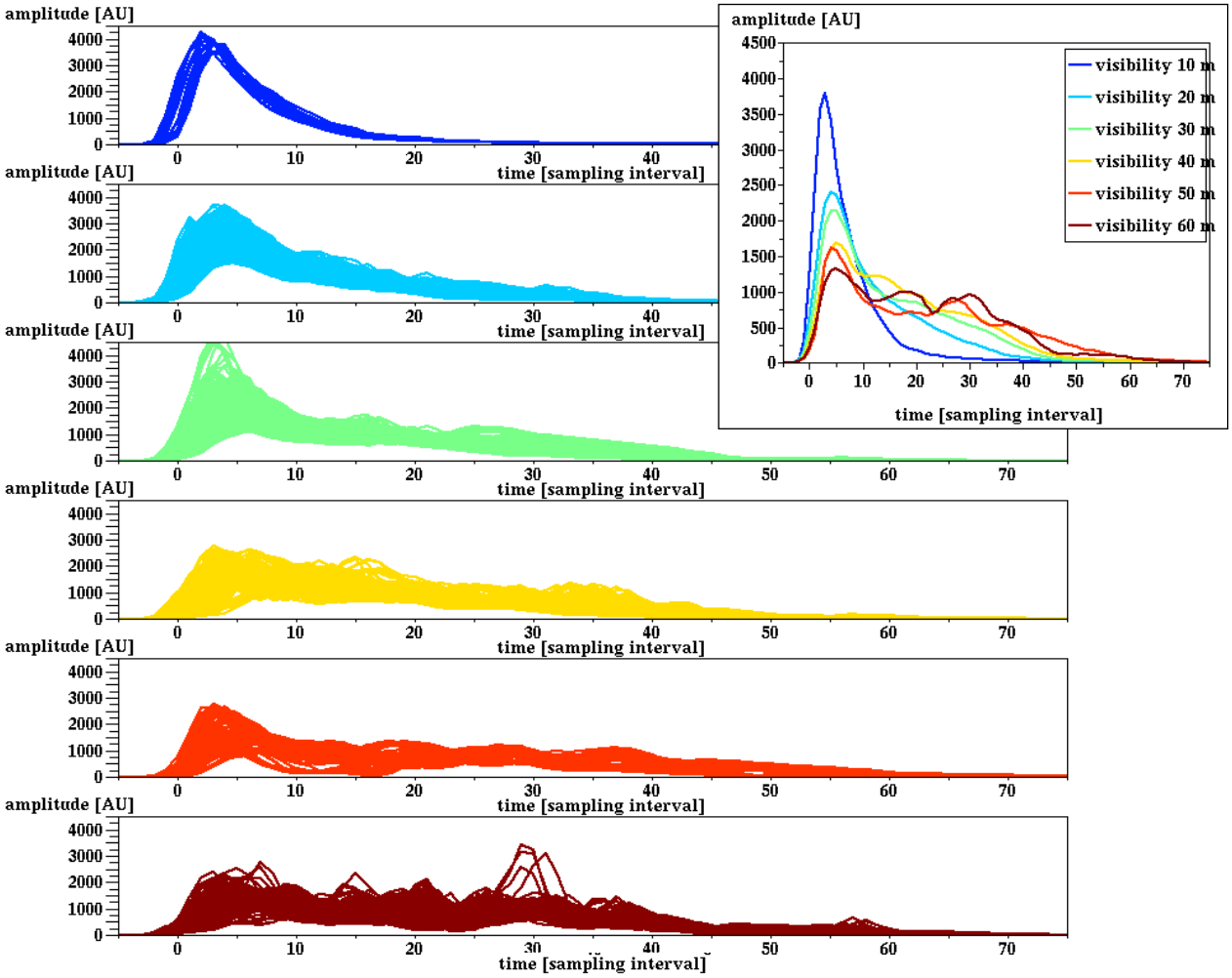

Figure 7: Waveforms resulting from the fog for 6 different visibility ranges. The insert provides the corresponding mean waveforms for comparison in one single chart.

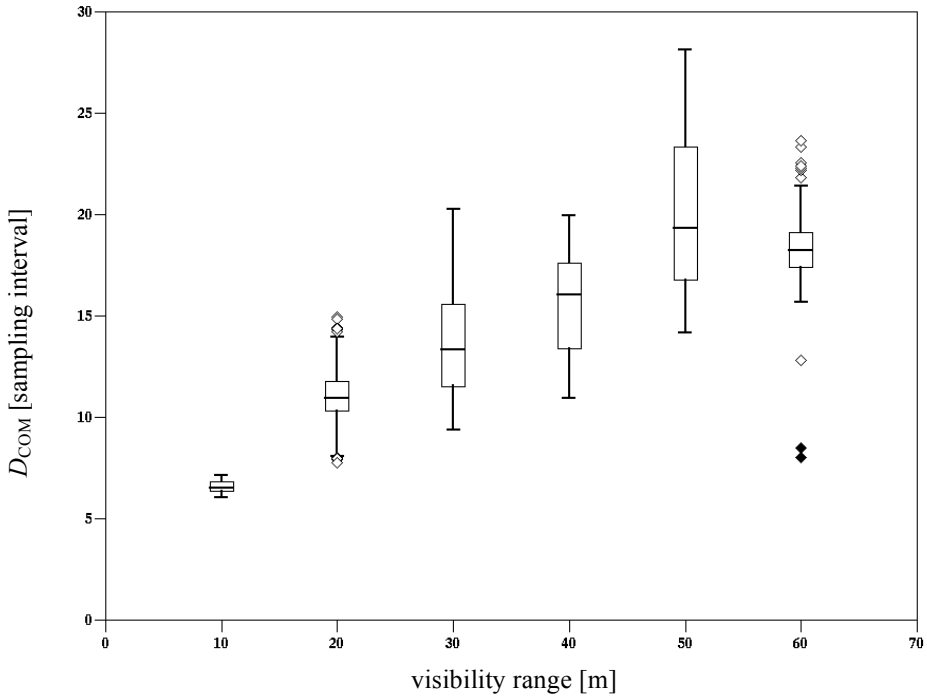

Figure 8: Boxplot of the distance between the position of the center of mass and the rising edge, D_{COM} of the fog's echo waveform versus the visibility range. In total about 1000 waveforms have been analyzed. The bottom and top of the boxes correspond to the first and third quartile, the whiskers refer to the data within 1.5 times the interquartile range (IQR). The white and black diamonds correspond to outliers below and above 3 times the IQR.

6. CONCLUSION AND OUTLOOK

Experimental results obtained with a production *RIEGL* VZ-1000 in a fog chamber have been presented and the influence of the fog on the measurement results has been analyzed. It has been illustrated how the relative reflectance value can deliver correct values even in the presence of dense fog by correctly setting the visual visibility. Furthermore the results prove that suppressing targets from within the fog by filtering is possible by applying a threshold for the pulse shape deviation. With its multi-target capability, online waveform processing, and the rich set of valuable attributes of every point of the resulting point cloud, all RIEGL V-Line instruments show an outstanding performance in reliably surveying targets in fog, dust, and precipitation.

In the second part it was investigated if and how the visibility range might be estimated from the fog's echo waveform. It can be seen from the waveforms gathered in the course of the experiments that there is a quite distinct relation between the pulse shape and the visibility range. Lower visibility (i.e. more dense fog) corresponds to more confined waveforms as the attenuation and distributed reflection of the medium is so high that layers from further within cannot contribute to the medium's waveform response. From these findings it is proposed to determine the visibility range from the distance between the position of the center of mass and the rising edge of the fog's echo waveform. While this is quite uncertain for single measurements it may lead to a reliable estimation when averaging the result over a number of measurements.

There are a few open questions: The first is how waveforms resulting from different sorts of turbidity would look like. It is unknown if the observed inhomogeneity of fog when less dense is a property of the experimental setup or an inherent property of fog. Furthermore it would be interesting to see if the scaling factor for the atmospheric attenuation determined in the course of the experiments would be equal for e.g. sand clouds. Finally it is open for further investigations if and how the findings may be used to perform a reliable estimation of the visibility range in real time.

REFERENCES

[1] RIEGL Laser Measurement Systems GmbH, Online: www.riegl.com (2014).

[2] Pfennigbauer, M., Rieger, P., Studnicka, N., Ullrich, A., "Detection of concealed objects with a mobile laser scanning system". Proc. SPIE 7323 (2009).

[3] Pfennigbauer, M., Ullrich, A., "Improving quality of laser scanning data acquisition through calibrated amplitude and pulse deviation measurement", Proc. 7684, 76841F-1 - 76841F-10 (2010).

[4] Pfennigbauer, M., Wolf, C., Ullrich, A., "Enhancing online waveform processing by adding new point attributes ", Proc. SPIE 8731 (2013).

[5] Pfennigbauer, M., Ullrich, A., "New point attributes from online waveform processing", ILMF Denver (2014).

[6] Mandlburger, G., Pfennigbauer, M., Pfeifer, N., „Analyzing near water surface penetration in laser bathymetry - A case study at the River Pielach", ISPRS Workshop Laser Scanning 2013, Antalya, Turkey (2013).

[7] Wagner, W., "Radiometric calibration of small-footprint full-waveform airborne laser scanner measurements: Basic physical concepts", ISPRS Journal of Photogrammetry and Remote Sensing, 65, 505-513 (2010).

[8] Ullrich, A., Pfennigbauer, M., "Echo Digitization and Waveform Analysis in Airborne and Terrestrial Laser Scanning", 53rd Photogrammetric Week, Stuttgart (2011).

[9] Roncat, A., Bergauer, G., Pfeifer, N,. "B-spline deconvolution for differential target cross-section determination in full-waveform laser scanning data" ISPRS Journal of Photogrammetry and Remote Sensing, 66, 418–428 (2011).

[10] Wagner, W., Ullrich, A., Ducic, V., Melzer, T., Studnicka, N., "Gaussian decomposition and calibration of a novel small-footprint full-waveform digitising airborne laser scanner. ISPRS Journal of Photogrammetry and Remote Sensing", 60(2), 100–112 (2006).

[11] Hug, C., Ullrich, A., Grimm, A.: Litemapper-5600. A waveform-digitizing LIDAR terrain and vegetation mapping system. International Archives of Photogrammetry, Remote Sensing and Spatial Information Sciences, 36 (Part 8/W2), 24 – 29 (2004).

[12] Jelalian, A.V., "Laser radar systems," Artech House, Boston London (1992).

[13] RCA Corporation, "Electro-Optics Handbook", RCA Commercial Engineering, Harrison (1974).